Catalysis Today 148 (2009) 140–147

Contents lists available at ScienceDirect

Catalysis Today

journal homepage: www.elsevier.com/locate/cattod

Use of different mesostructured materials based on silica as cobalt supports for the Fischer–Tropsch synthesis

O. González [a,*], H. Pérez [b], P. Navarro [b], L.C. Almeida [b], J.G. Pacheco [c], M. Montes [b]

[a] Energy Unit, INASMET-TECNALIA, Mikeletegi Pasealekua, 2 Parque Tecnológico, E-20009 San Sebastián, Spain
[b] Department of Applied Chemistry, University of the Basque Country, P° Manuel de Lardizábal, 3 E-20018 San Sebastián, Spain
[c] División Académica de Ciencias Básicas, Universidad Juárez Autónoma de Tabasco, Km 1 – Carretera Cunduacán – Jalpa de Méndez, A. P. 24, C.P. 86690, Cunduacán, Tabasco, México

ARTICLE INFO

Article history:
Available online 5 May 2009

Keywords:
Fischer–Tropsch synthesis
SBA-15
Al-MCM-41
INT-MM1
Mesoporous support
Supported cobalt catalysts

ABSTRACT

To obtain a novel, active and selective to diesel catalytic material for syngas processing via Fischer–Tropsch synthesis (FTS), a series of 20 wt.% cobalt catalysts has been prepared by impregnation of a mesoporous molecular sieve based on silica (SBA-15, Al-MCM-41, INT-MM1), and a commercial amorphous silica for comparison purposes. All materials were characterized by several physico-chemical techniques: AAS, BET surface area, XRD, TPR, and H_2 chemisorption with pulse reoxidation and finally their reactivity on the FTS reaction was evaluated at 523 K, 10 bar, and $H_2/CO = 2$. Catalytic and characterization results show a great influence of mesoporous support porosity on the structure, reducibility, and FTS catalytic behavior of cobalt oxide species supported over these ordered materials. It was found that the size of supported cobalt oxide species formed during the calcination step increased with the average pore size (D_p) of the mesoporous support. Thus, the catalyst with larger Co oxide species located in wide pore silica showed to be easily reducible, more active and very selective toward the diesel fraction. It seems to be the case of the Co/SBA-15 solid, which showed to be the most active solid (XCO ~63%) when the same mass of catalyst was used. Under CO iso-conversion conditions (XCO ~40%), Co/SBA-15 was more selective toward the formation of C_{5+} hydrocarbons (~80%, $\alpha = 0.76$) and less selective to CH_4 (~15%). On the contrary, when Al-MCM-41 and INT-MM1 were used as supports, a lower selectivity to C_{5+} and CO conversion and higher CH_4 selectivity (~20%) were observed due to the decrease of D_p, of the cobalt oxide species size and the reducibility degree of such species.

1. Introduction

Fischer–Tropsch synthesis (FTS) is a part of gas-to-liquids (GTL) technology, which produces synthetic liquid hydrocarbons from natural gas. Recently the production of clean fuels and particularly of synthetic diesel by means of the FTS process has aroused renewed interest in both industrial and academic field [1–3]. The super clean diesel oil fraction produced through the FTS is mainly composed by linear paraffins having high cetane numbers (>70) and it is free of sulfur and aromatics pollutants. The quality of this diesel offers significant environmental and efficiency benefits over those derived from crude oil [4].

The FTS is a surface-catalyzed polymerization process that uses CH_x monomers, formed by hydrogenation of adsorbed CO, in order to produce hydrocarbons with a broad range of chain length and functionality. This process was shown to be catalyzed by certain transition metals, such as Co, Fe and Ru, which present the highest activity [5,6]. Among them, Co is considered the most favourable metal for the synthesis of long-chain hydrocarbons from synthesis gas due to its high activity per weight of metal compared to Fe, high selectivity to linear paraffins, high stability toward deactivation by water (a by-product of the FTS process), low water–gas shift activity and low price compared to noble metals such as Ru, Re, or Pt [6,7].

In the FTS process it has been shown that both catalyst activity and hydrocarbon selectivity are function of the density of surface-active sites (Co^0), and at the same time depend on both cobalt dispersion and reducibility [7,8]. These two parameters are mainly determined by the cobalt-support interaction strength [8,9]. In order to achieve a high density of metal sites (Co^0), cobalt precursors are usually dispersed on porous carriers, such as amorphous SiO_2, Al_2O_3, or TiO_2. A large number of publications have shown that the nature of the metal precursor [1,10,11], the conventional carriers [1,12–16] the preliminary treatments [1,3,17,18] and the metal loading [1,7,10,19] could significantly influence the extent of metal reduction, morphology, adsorption

* Corresponding author. Tel.: +34 943 003700; fax: +34 943 003800.
E-mail address: orlando.gonzalez@inasmet.es (O. González).

0920-5861/$ – see front matter © 2009 Elsevier B.V. All rights reserved.
doi:10.1016/j.cattod.2009.03.030

and catalytic properties of the active phase, especially in well-dispersed catalysts. In addition to the effects of these parameters, others studies have shown that the support porous structure can strongly affect Co dispersion, Co reducibility and FTS catalytic performance of supported cobalt catalysts [16,20,21]. Therefore, the choice of a support is a very important aspect for the final design of new FTS catalysts, since it not only determine the number of active sites stabilized after reduction pretreatment, but it can also influence the amount of cobalt oxide species that can be reduced [1,8,22].

In this sense, the use of mesostructured materials based on silica (MCM-41 and SBA-15 [12,20,23–25], and HMS [26]) and zeolitic materials (ITQ-2 and ITQ-6 [8], ZSM-5, NaY and HY [25]) as supports for preparing Co-based FTS catalysts has been explored in the last decade, since these materials represent an efficient tool to control the sizes of supported cobalt particles [18,27]. On the one hand, the typical very high surface area of these mesoporous molecular sieves should allow higher dispersions at higher Co loadings compared to amorphous silica. On the other hand, the presence of a uniform pore size distribution in the ordered mesoporous materials should allow a better control on the cobalt crystallite size and thus on the catalytic properties. Besides, narrow pore size distribution of the support could prevent the sintering effect of the cobalt particles.

Nowadays the use of periodic mesoporous silica as supports for heterogeneous metal catalysts has caused a great interest in a wide range of catalytic reactions: photocatalysis, hydrogenation, hydrodesulfurization, oxidative dehydrogenation and more recently FTS. The utilization of such novel materials as supports of Co catalysts makes it possible to design new catalysts with higher productivity for C_{10}–C_{20} paraffins as the main component of diesel oil.

In this work, a series of mesoporous molecular sieves based on silica, such as: SBA-15, Al-MCM-41, and INT-MM1 (a novel material) with different average pore diameters (D_p) and high surface areas (>730 m^2/g) has been studied as supports of cobalt catalysts (~20 wt.% Co) to be tested in FTS. The obtained results were compared to commercial amorphous silica. MCM-41 materials are usually synthesized in a basic medium in the presence of surfactants [28]. The D_p of MCM-41 materials may vary from 2 to 10 nm as a function of the alkyl chain length of the surfactant template and synthesis conditions. SBA-15 materials are typically prepared in acid conditions with poly (alkyl oxide) tri-block copolymers [29,30]. They usually have wider pores (up to 30 nm) and thicker walls than MCM-41. Both solids have periodically ordered structures, which consist of two-dimensional arrays of uniform mesopores; the pore size distributions in these periodic mesoporous silicas are very narrow.

The mesoporous material INT-MM1, a novel molecular sieve developed by PDVSA–INTEVEP S.A. [31], is an inert material based on silica. It has a high BET surface area and good thermal and hydrothermal stability. It presents tortuous channels of uniform diameter (~2.5 nm) with short-range order and high concentration of hydroxyl groups on its surface, which facilitates the incorporation of dispersed metal phases. This material has a bimodal pore distribution, with pore volume $V_p > 0.2$ mL/g. It is synthesized using conventional sol–gel methods. Among other applications, this material has been used as a selective adsorbent of polluting molecules in liquid streams, as a catalyst support in hydrocarbon selective oxidation, hydrotreatment reactions, fine chemistry, dry reforming [32] and for the first time in FTS.

This work focuses on the effect of support mesoporous structures on the cobalt dispersion and its reducibility, and how these parameters influence on the product distribution and catalytic behavior of the Co catalysts tested in FTS reaction.

2. Experimental

2.1. Preparation of catalytic materials

The parent silica SBA-15 and Al-MCM-41 materials were synthesized in the laboratory following a procedure involving an initial stage of silica-surfactant self-assembly and other stage of large hydrothermal treatment according to [30,33], respectively. SBA-15 silica was synthesized in acidic media using Pluronic triblock copolymer (EO_{20}–PO_{70}–EO_{20}, P123, Aldrich) as the structure-directing agent (surfactant) and tetraethyl orthosilicate (TEOS, Aldrich, 99 wt.%) as Si source. The Al-MCM-41 mesoporous sieve was synthesized in basic media from SiO_2 + $AlO(OH)_2$ [33]. In this synthesis, the silicon oxide (Baker, ~100% purity) was used as Si source, the boehmite (Catapal B from Sasol, Germany) was used as Al source and the hexadecyltrimethylammonium bromide (CTMABr, Aldrich, 99 wt.%) was used as surfactant (templating agent). The synthesis of the material was initiated by mixing and stirring of an aqueous solution of surfactant with an aqueous solution consisting of tetramethylammonium hydroxide (TMAOH, Aldrich 97 wt.%) containing the Si source. Afterward, the amount of boehmite necessary to reach a mol ratio Si/Al = 100 in the final material was added. The aluminum incorporation to the MCM-41 matrix during the step of hydrothermal synthesis has the objective of improving the thermal and hydrothermal stability of this material, since the structure of MCM-41 has been reported to collapse after brief heating in boiling water [3,34]. The INT-MM1 mesoporous material has been supplied by PDVSA–INTEVEP S.A., and it was prepared according to the method patented by Carraza et al. [31]. The commercial amorphous silica, Kali Chemie AF125 was used as support for comparison purposes.

All catalysts with a Co loading ~20 wt.% were prepared by incipient wetness impregnation using a solution of $Co(NO_3)_2{\cdot}6H_2O$ (Aldrich, 98% purity) dissolved in excess of ethanol with respect to the pore volume of each silica material used as support (liquid/solid ratio ~5 cm^3/g), followed by slow evaporation of the solvent in a rotary evaporator at 35 °C until dryness. Afterward, the samples were further dried at 60 °C overnight and milled at 250 r.p.m. for 15 min by means of a centrifugal ball mill. Finally, the catalysts were calcined in air at 350 °C for 6 h by increasing the temperature at a controlled heating rate of 2 °C/min.

2.2. Characterization techniques

The metal content in the calcined samples was determined by atomic absorption spectrophotometry (AAS) using a GBC Avanta ε equipment.

The N_2 adsorption–desorption isotherms were measured at −196 °C on a Micromeritics ASAP 2020 volumetric system, with the samples previously outgassed for ~8 h at 120 °C. The surface areas (S_{BET}) of silica supports and Co catalysts were determined by the BET method. The total pore volume (V_p) was calculated from the amount of vapor adsorbed at a relative pressure (P/P_0) close to unity. Pore size distribution was established from the adsorption branches of the isotherms using BJH method.

XRD patterns were obtained at room temperature in a Bruker D8-Advance X-ray diffractometer using a graphitic monocromator and a Cu Kα-ray radiation (λ = 1.540598 Å) operating at 40 kV and 30 mA. The sweeping used for all the samples was from 5° to 85° with step size of 0.05° at an interval of 100 s. The Co_3O_4 average crystallite size was calculated using the Scherrer equation [35] for the more intense peak (2θ = 36.8°).

TPR profiles were obtained using a TPD/R/O 1100 equipment of ThermoFinnigan. About 17 mg of calcined catalyst was placed in a quartz tubular reactor and then a mixture of 5.11% H_2 in Ar was passed through the sample at a total flow rate of 20 mL/min while

the temperature was increased from 35 to 1100 °C at a heating rate of 10 °C/min.

H_2 chemisorption was conducted using temperature-programmed desorption (TPD) with the TPD/R/O 1100 equipment under experimental conditions previously reported [36,37]. A sample of about 0.250 g was activated using a H_2 flow of 30 mL/min at 350 °C for 10 h and then cooled to 100 °C keeping the initial flow conditions. The sample was kept at 100 °C for 90 min under argon flow (30 mL/min) to remove and/or prevent adsorption of weakly bound H_2 species. Afterward, the H_2 TPD profile was obtained increasing the temperature from 100 to 350 °C for 1 h using a heating rate of 10 °C/min under argon flow. The TPD profile was integrated and the number of moles of desorbed hydrogen was determined making comparison of the obtained area with the areas of calibrated hydrogen pulses. Dispersion calculations were based on the assumption of 1:1 H:Co stoichiometric ratio, taking into account the fraction of reduced Co particles [36,37]. The cobalt metal crystallite size was estimated from the cobalt dispersion by assuming spherical and uniform cobalt metal particles [38]. To estimate the Co dispersion ($D_{\text{corrected}}$%) and the Co^0 crystallite size, d (Co^0), the Eqs. (1) and (2) were used:

$$D_{\text{corrected}}(\%) = \frac{\text{number of Co}^0\text{ atoms on surface}}{\text{total Co atoms in samples} \times \text{reduced Co fraction}} \times 100 \quad (1)$$

$$d(\text{Co}^0)\,(\text{nm}) = \frac{96}{D_{\text{corrected}}(\%)} \quad (2)$$

After TPD of hydrogen, the sample was reoxidized at 350 °C using pulses of oxygen. The reduced cobalt fraction was calculated by assuming that the Co^0 was completely reoxidized to Co_3O_4 [36,37].

2.3. Catalytic measurements

Standard catalytic tests were carried out in a *Microactivity Reference* equipment (PID Eng&Tech. S.L.) [39]. About 0.45 g of catalyst were used with a total flow adjusted to assure a space velocity of 0.15 mol kg^{-1} s^{-1} using a feed of $N_2/H_2/CO$ (9/60/30) corresponding to a H_2/CO ratio of 2. Total pressure was fixed to 10 bar, the reaction temperature at 250 °C and the reaction time to 70 h. Prior to the catalytic tests the catalysts were reduced in situ at atmospheric pressure using a flow of 54 mL/min of H_2 at 350 °C for 10 h. During the reaction, the reactor effluent passed through a hot trap kept at 120 °C and 10 bar to collect waxes. The previously depressurized gaseous products were sent through a thermostatic line at 200 °C to a two-ways 6890 Agilent GC, using a FID to analyze hydrocarbons from C_5 to C_{18} and a TCD to analyze permanent gases and light hydrocarbons.

3. Results and discussion

3.1. Textural properties of materials

The nitrogen adsorption–desorption isotherms for the siliceous supports, with the corresponding pore size distribution curves calculated using BJH method are shown in Figs. 1a and 2a, respectively. The estimated textural parameters such as: S_{BET}, V_p and D_p for siliceous supports and their corresponding Co-supported catalysts are shown in Table 1. According to the classification of Brunauer et al. [40], all supports based on mesoporous silica (see Fig. 1a) presented a type IV isotherm and only for the SBA-15 and MCM-41 supports a reversible part and a type H1 hysteresis loop were observed at higher relative pressures,

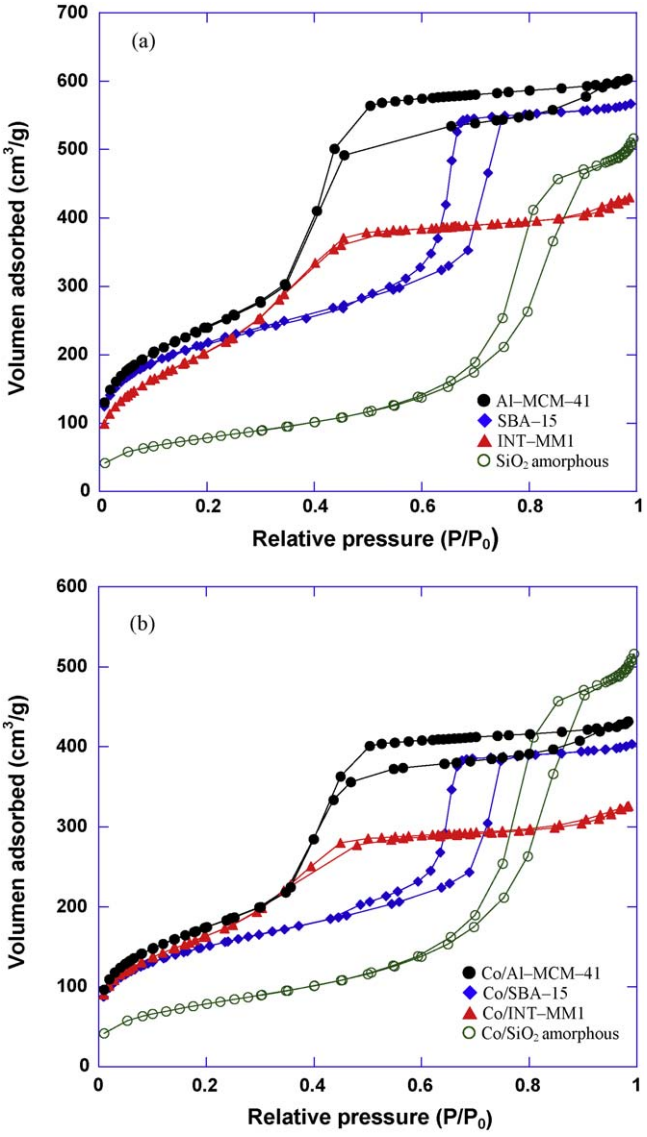

Fig. 1. Nitrogen adsorption–desorption isotherms obtained at −196 °C for: (a) supports based on silicas and (b) Co catalysts supported on silica supports.

associated with the presence of cylinder shape pore of rather constant cross-section [40,41]. The shapes of these isotherms are typical for mesostructured materials and occur on porous adsorbents possessing pores in the diameter range from 2 to 50 nm. The isotherms for the SBA-15 presented a sharp inflection in the range of relative pressure from 0.7 to 0.8 (see Fig. 1a) indicative of good-quality SBA-15 material with uniform mesopores [7,42]. On the other hand, the shape of the adsorption–desorption isotherms for the Kali Chemie AF125 commercial silica presented a sharp inflection in the range of relative pressure from 0.8 to 1.0 with hysteresis loop. This reveals a wide pore size distribution that corresponds to a macroporous material.

Although the BJH pore sizes distribution curves for the SBA-15 and Co/SBA-15 solids show a mesopore bimodal distribution in Fig. 2a and b, respectively, it is important to clarify that the smaller peaks observed around 4 nm are the result of a physical phenomena known as the tensile strength effect [43]. Nevertheless, it is well known in the literature that the SBA-15 material also present microporosity [7]. Additionally, the curves in Fig. 2a shows a uniform and narrower pore size distribution for the SBA-15 support compared to the rest of mesoporous silicas. On the

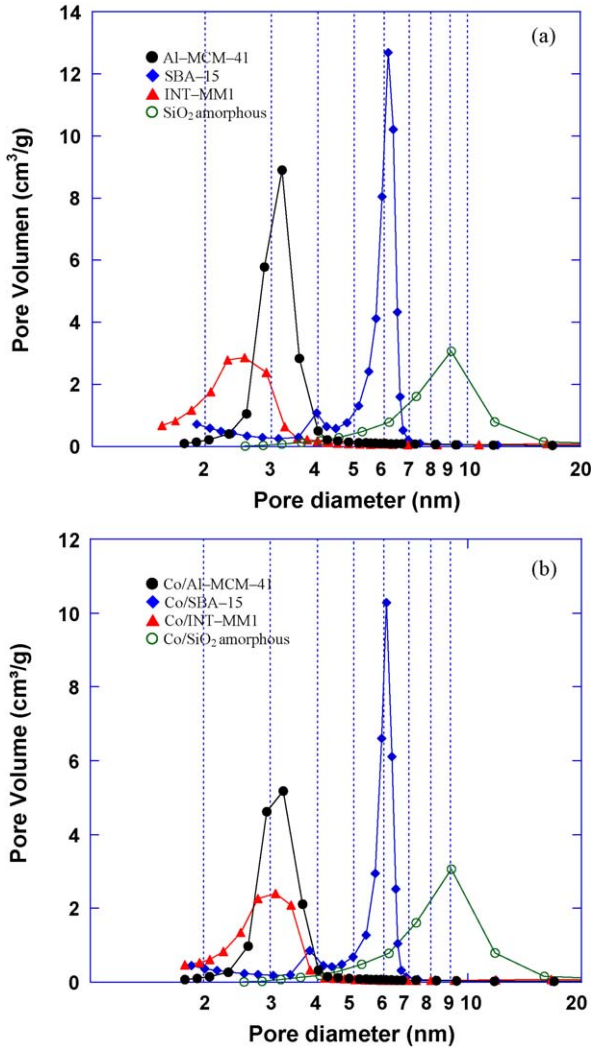

Fig. 2. BJH pore size distribution curves calculated from nitrogen desorption isotherms of: (a) supports based on silicas and (b) Co catalysts supported on silica supports.

other hand, the N_2 adsorption–desorption isotherms for the INT-MM1 support and the Al-MCM-41 modified mesoporous silica (see Fig. 1a) practically did not show hysteresis loop in agreement with that previously reported for these materials [31,33]. For Al-MCM-41, the sharp increase observed in adsorbed volume at 0.3–0.4 relative pressure followed by a plateau indicates capillary condensation within mesopores in a narrow diameter range (see Fig. 2a).

The absence of hysteresis in the isotherms of the INT-MM1 support (see Fig. 1a) indicates that the channels in the material are formed by a uniform system of through-pores (open at both ends) that are interconnected. The shape of these isotherms is typical for this type of mesoporous material [31]. Previous results obtained from the density function theory (DFT) method for the INT-MM1 gave an D_p of 2.5 nm and a bimodal pore distribution, with approximately 55% mesoporosity and 45% microporosity contributing to the total surface area of this material [31]. The bimodal pore supports, such as SBA-15 and INT-MM1 contain large and small pores simultaneously. The small pores could yield the sites for anchoring smaller cobalt oxide particles, while the large pores could provide a network for fast diffusion of reacting molecules and products.

The nitrogen adsorption–desorption isotherms for the catalysts: Co/Al-MCM-41, Co/SBA-15, Co/INT-MM1 and Co/SiO_2 (amorphous) and the corresponding pore size distribution curves calculated using BJH method are shown in Figs. 1b and 2b, respectively. The shapes of the N_2 adsorption isotherms of Co-supported samples were quite similar to their corresponding siliceous supports (see Fig. 1a), suggesting that the mesoporous structure was mostly retained upon Co impregnation in all cases. This observation is in agreement with previous reports [44,45]. Also note that the shape of pore size distribution curves (Fig. 2b) remains the same, though the D_p of the catalysts was lightly smaller after cobalt introduction, except for INT-MM1, which presented an increase from 2.6 to 3.1 nm (see Table 1, and Fig. 2a and b). This increase may be caused by both partial collapse of its mesoporous structure as a consequence of its low pore wall thickness (≤1.7 nm) compared with the Al-MCM-41 (∼1.7 nm) and SBA-15 (∼5.4 nm) supports [12,26,31], and/or the partial degradation of pure silica matrix caused by the presence of high concentrations of hydroxyl groups in INT-MM1. The interaction of these hydroxyl groups with the humidity in time could facilitate the hydrolysis of silica matrix, especially when the INT-MM1 lote used has been stored during several years.

The chemical analysis results are presented in Table 1. Nominal and real cobalt contents were very similar. Cobalt introduction on supports based on silica leads to a sharp decrease in S_{BET} in all cases. The S_{BET} in all periodic mesoporous silicas (Al-MCM-41, SBA-15, and INT-MM1) was higher than 730 m^2/g, whereas the S_{BET} of the commercial amorphous silica was much lower (280 m^2/g).

Table 1
Chemical and physical properties of supports based on silica and Co-supported catalysts calcined at 350 °C.

Samples	Co content (wt.%)	Textural properties[a]						Structural properties			
		D_p[b] (nm)		V_p (cm^3/g)		S_{BET}[b] (m^2/g)		Co dispersion (%)	Co^0 crystallite size (nm)	Reduced Co fraction (%)	Co_3O_4[c] average crystallite size (nm)
		Fresh[d]	Used[e]	Fresh[d]	Used[e]	Fresh[d]	Used[e]				
SBA-15	–	4.9		0.87		781		–	–	–	–
Al-MCM-41 (Si/Al) = 100	–	3.2		0.93		860		–	–	–	–
INT-MM1	–	2.6		0.66		730		–	–	–	–
SiO_2 amorphous	–	8.4		0.79		280		–	–	–	–
Co/SBA-15	18.1	4.8	5.1	0.62	0.20	538	205	3.0	32.6	81	14.6
Co/Al-MCM-41	17.7	3.2	3.4	0.66	0.23	625	212	5.3	18.1	44	7.0
Co/INT-MM1	20.9	3.1	3.6	0.50	0.15	584	170	4.7	20.3	36	6.8
Co/SiO_2	19.3	8.1	8.3	0.54	0.36	209	136	2.1	45.8	94	14.9

[a] Values obtained from N_2 adsorption–desorption isotherms.
[b] D_p and surface area values obtained by means of the BJH and BET methods, respectively.
[c] Values calculated using the Scherrer equation for the more intense peak ($2\theta = 36.8°$).
[d] Calcined samples.
[e] Used samples in FTS for 70 h on stream.

Compared to the pure mesoporous silicas, a reduction of S_{BET} and V_p is noted for all catalysts after incorporation of ~20 wt.% Co. The decrease may be attributed to the dilution effect of the support caused by the presence of the supported cobalt oxide phase, and/or to a partial blockage of the support pores (specially micropores and mesopores) occurred after Co incorporation [7,20].

Textural properties comparison between the fresh and used catalysts has been performed in order to evaluate their hydrothermal stability. In Table 1 are also listed the textural properties of the used catalysts in FTS after 70 h on stream, where a slight increase in D_p and a sharp decrease in S_{BET} and V_p were observed again. These observed variations suggest that the ordered structure of these mesoporous materials under reaction conditions continue collapsing in varying degree depending on their hydrothermal stability and therefore depending on the pore wall thickness of mesoporous material. Thus, according to the differences between D_p, S_{BET} and V_p noticed for fresh and used catalysts might be established a hydrothermal stability order for all mesoporous materials as follows: Co/SBA-15 > Co/Al-MCM-41 > Co/INT-MM1. The observed variations in D_p, S_{BET} and V_p could be also attributed to the accumulation of the waxes deposited in the catalyst pores.

3.2. X-ray diffraction: cobalt species and crystallite sizes

The XRD patterns for all cobalt catalysts supported on mesoporous silicas are presented in Fig. 3. These show five sharp signals characteristic of Co_3O_4 spinel (PDFWIN 42-1467) and one broad signal with low intensity located at $2\theta = 23^\circ$ typical of siliceous materials. The latter signal is attributed to diffuse dispersion caused by the lack of long-range order of Si atoms located on the walls of the channels in the materials based on silica.

The XRD peaks become narrower and more intense for the Co/SiO_2 and Co/SBA-15 catalysts, indicating the presence of larger and easier to reduce Co_3O_4 crystallite size in these materials in comparison with the Co/Al-MCM-41 and Co/INT-MM1 solids. This observation can be correlated with the Co_3O_4 average crystallite size data and the results of reduced Co fraction presented in Table 1, where is clearly showed that the Co/SiO_2 and Co/SBA-15 samples exhibit the largest Co_3O_4 average crystallite size (~15 nm) and the higher reduced Co fraction (>80%). In this sense, strong metal-support interactions and consequently higher Co dispersion percentages are expected to be found in the Co/Al-MCM-41 and Co/INT-MM1 catalysts.

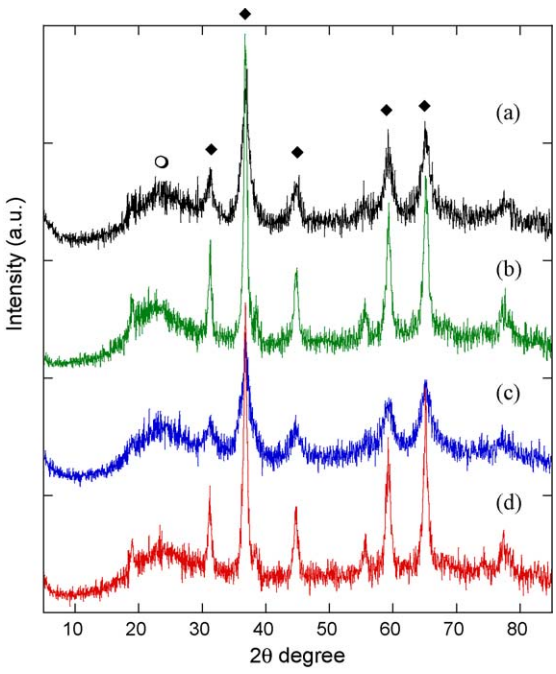

Fig. 3. XRD patterns of cobalt-supported catalysts. (a) Co/Al-MCM-41, (b) Co/SiO_2 amorphous, (c) Co/INT-MM1, and (d) Co/SBA-15. Identified phases: (○) amorphous SiO_2 and (◆) Co_3O_4 spinel.

On the one hand, Table 1 shows that the sizes of the supported Co_3O_4 crystallites depend on silica porous structure, specifically from D_p since larger Co_3O_4 crystallite sizes are found in the catalysts prepared from the support with wider pores (SBA-15 and commercial SiO_2) and vice verse (Al-MCM-41 and INT-MM1). On the other hand, Table 1 also shows in all cases that the Co_3O_4 crystallite size values estimated for the catalysts exceed the D_p values calculated for their corresponding supports. Therefore, these results suggest that a portion of larger Co_3O_4 particles could be located on the external surface of the support while another portion (the smallest ones) could be encapsulated inside the mesoporous channels. This statement is consistent with previous works [7,8,20]. Additionally, those small Co_3O_4 particles in narrow pores are expected to be more difficult to reduce than those larger ones deposited in wider pores, suggesting in a certain sense that differences in Co_3O_4 crystallite sizes lead to differences in Co reducibility. This argument is in line with the reduced Co fraction results shown in Table 1 and with the results previously reported by other authors [1,20,46].

It must be noted that in Table 1 are shown notable differences between the Co_3O_4 average crystallite size values obtained for all the catalysts and their corresponding Co^0 crystallite size values. In all cases the second ones values are larger than the first ones. These discrepancies could be explained by sintering effects of reduced metal species and/or by considering the limitations and approximations of the characterizations techniques used for this type of analysis.

3.3. Temperature-programmed reduction: cobalt species reducibility

Fig. 4 shows TPR profiles of the supported cobalt oxide particles on the different mesoporous supports based on silica. As observed, all the samples exhibit two main reduction peaks with a maximum located in the temperature ranges 290–315 and 320–370 °C, which correspond to the two-step reduction process in which the Co_3O_4 phase is first reduced to CoO and then the CoO phase is reduced to Co^0 [36,37]. The TPR profiles for the Co/SiO_2 and Co/SBA-15 catalysts (see Fig. 4b and d, respectively) are quite similar, indicating a comparable reducibility degree of the supported oxide species on them as can be corroborated by the reduced Co fraction results shown in Table 1. These catalysts presented very similar Co_3O_4 average crystallite sizes (~15 nm) despite they showed very different D_p and Co dispersion values. Thus, periodically ordered structures based on silica used as Co catalyst support lead to higher metal-support interactions compared to amorphous silica. Others no identified supported cobalt oxide species with smaller crystallite sizes and lower reducibility degree can be observed at temperature above 400 °C. This variety of surface-Co oxide species is represented by several shoulders and peaks of reduction showed in the temperature range from 400 to 1000 °C (see Fig. 4). The interaction degree of these surface-Co oxide species with the support is directly proportional to the temperature increase and inversely proportional to their crystallite sizes. According to this argument, the Co/SBA-15 solid (see Fig. 4d) exhibits two unique Co oxide species not observed on the rest of the samples: a reduction feature with a maximum at 432 °C and a small shoulder at 600 °C. These signals could be attributed to easily reducible surface-Co species at the reduction conditions, which could be responsible for the catalytic behavior experimentally observed for this sample, as will be hereinafter discussed. In the same way, the Co/Al-MCM-41

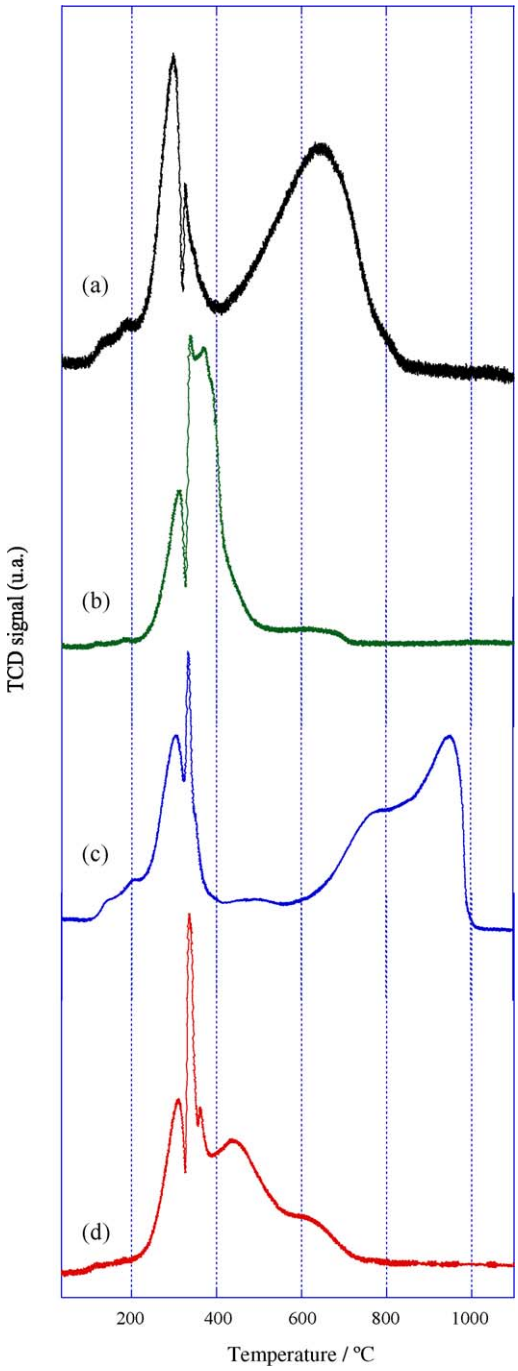

Fig. 4. TPR profiles of cobalt-supported catalysts. (a) Co/Al-MCM-41, (b) Co/SiO_2 amorphous, (c) Co/INT-MM1, and (d) Co/SBA-15.

solid (see Fig. 4a) presents a broad and intense reduction peak with a maximum located at 664 °C, which could be attributed to the reduction of the small surface-cobalt particles strongly interacting with the support. For the rest of the solids, this signal was not observed either. For the case of the Co/INT-MM1 solid (see Fig. 4c), a shoulder at 800 °C and an intense reduction feature with maximum hydrogen consumption were observed above 952 °C, most likely corresponding to the reduction of very small cobalt silicate particles, which are stable and difficult to reduce and to detect by XRD measurements. It has been reported that during the reduction process the cobalt silicate phases formed probably can be produced by reaction of highly dispersed CoO phases with the support based on silica [8,47]. The formation of hardly reducible cobalt species in this case could be attributed to the CoO-support interaction produced as a consequence of very small cobalt particles confined inside the mesoporous channel of this material. For this reason, the INT-MM1 silica is a least appropriated material to be used as Co catalyst support.

The cobalt reduction degree determined by reduced fraction measurements for the Co-supported catalysts is presented in Table 1. The obtained results are in good agreement with the TPR profiles discussed above. According to this, the reducibility order observed in Fig. 4 based on the ease of reduction of these materials was as follows: $Co/SiO_2 > Co/SBA\text{-}15 > Co/Al\text{-}MCM\text{-}41 > Co/INT\text{-}MM1$. Thus, a high reduction degree was obtained for Co/SBA-15 (>80%, see Table 1) compared to the rest of mesoporous silicas. This suggests that a considerable portion of Co^0 small particles could be stabilized by the structure of own support. It is possible that the porous structure of the SBA-15 material prevents the sintering of the metallic phases due to the array and dimensions of its channels and to the metal-support interactions that could take place.

3.4. Fischer–Tropsch synthesis results: catalytic behavior

The results of activity in terms of syngas conversion (XCO%) and selectivity in terms of hydrocarbon product distribution (C_{5+}) and chain growth probability (α) are shown in Table 2. As observed, when ~0.4 g of each catalyst were used under the same FTS reaction conditions, the Co/SBA-15 catalyst displayed the highest CO conversion (~63%) than the rest of catalysts tested, showing very similar selectivity results ($\alpha \sim 0.70$ and selectivity to C_{5+} between 71 and 74%). It is well known that FTS selectivities could be affected by conversion. For this reason, the selectivities should be compared at similar conversion levels to evaluate any changes arising from differences in catalysts properties. In this sense, under CO iso-conversion conditions (~40%) the Co/SBA-15 mesoporous catalyst exhibited the highest selectivity to C_{5+} (~80%) and lowest selectivity to CH_4, with a higher α value than the rest of the tested solids in FTS reaction ($\alpha = 0.76$). The high activity and selectivity obtained for the Co/SBA-15 catalyst can be explained by the interplay between the reducibility obtained for this catalyst and its dispersion degree, which could be controlled by the pore size of the Co/SBA-15 support. A relation between the sizes of Co_3O_4 crystallites and extents of chain growth probability (α) on the pore diameters of mesoporous catalysts is presented in Fig. 5. According to the textural properties results (see Table 1 and Fig. 5), the Co/SBA-15 material presented the highest D_p (~5 nm) of the mesostructured material series evaluated in this work. The shape and dimensions of these pores could yield sites appropriated for the anchoring or encapsulating of surface-Co oxide species with sizes smaller than 5 nm. Such species could be easily reduced (81% of reducibility according results shown in Table 1) increasing the number of active sites available for the reaction, which can be reflected on a better catalytic performance.

Table 2
Catalytic activity and selectivity on Fischer–Tropsh synthesis.

Catalysts	XCO (%)	Selectivity (%)				
		CO_2	CH_4	C_2–C_4	C_{5+}	α^a
Co/SBA-15	63.2	0.9	22.3	5.7	71.1	0.70
Co/SBA-15	39.6[b]	0.3	15.6	4.5	79.6	0.76
Co/Al-MCM-41	38.5[b]	0.4	20.0	5.2	74.4	0.72
Co/INT-MM1	40.3[b]	0.7	21.2	6.3	71.8	0.70
Co/SiO_2	42.5[b]	0.5	22.1	6.0	71.4	0.70

Reaction conditions: $T = 250$ °C, $P = 10$ bar, $H_2/CO = 2$, GHSV = 0.15 mol kg^{-1} s^{-1}.
[a] Chain growth probability obtained from the approached expression $\alpha = (0.75 - 0.373)\sqrt{-\log(S_{C_{5+}})} + 0.25(S_{C_{5+}})$ [49].
[b] CO iso-conversion conditions closed to ~40%.

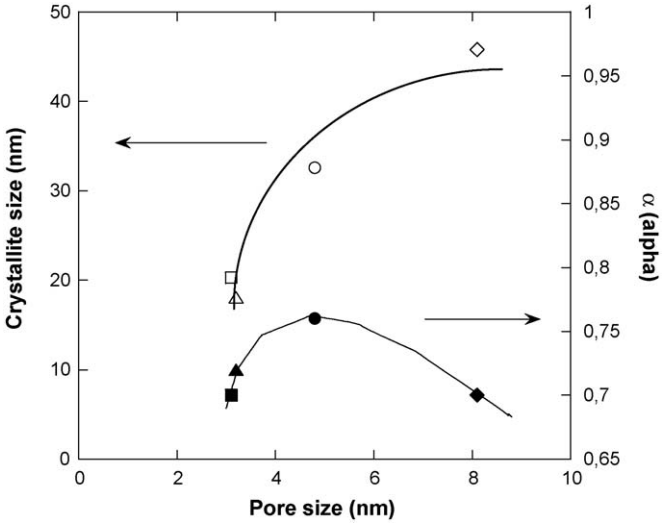

Fig. 5. Dependences of Co_3O_4 crystallite sizes and extents of chain growth probability (α) on the pore diameters of mesoporous catalysts: (▲△) Co/Al-MCM-41, (◆◇) Co/SiO_2 amorphous, (■□) Co/INT-MM1, and (●○) Co/SBA-15. α values determined under CO iso-conversion conditions (~40%).

It is worth noting that for a similar metal loading, product selectivities were comparable between the catalysts based on Al-MCM-41 and INT-MM1 mesoporous supports and the Co/SiO_2 reference solid, though a slightly higher selectivity to C_{5+} hydrocarbons was found for the Al-MCM-41-supported sample (see Table 2). In this case, the amorphous SiO_2 with a D_p of ~8 nm could lead to the formation of larger surface-Co oxide particles highly reducible (94% of reducibility according results shown in Table 1), but also susceptible to metal sintering process to cause larger Co^0 crystallite sizes (~46 nm, see Table 1). Unlike Co/SBA-15 mesoporous catalyst, similar results or no changes in terms of selectivity were expected for the Co/Al-MCM-41 and Co/INT-MM1 catalysts due to these materials presented very seemed D_p values (~3 nm). Therefore, the sizes of Co_3O_4 crystallites smaller than 3 nm formed in the pores of these materials (after calcining) led to the formation of small and seemed Co^0 crystallite sizes, which could be able to interact strongly with the support. This strong Co-support interaction yields a decrease in the extent of Co reduction (close to 40%, as seen in Table 1), which could lead to a decrease of Co^0 active sites necessary for improving the catalytic properties of these catalysts. Fig. 5 confirms this abovementioned argument, since it shows no changes in crystallites sizes and values of α for the Co/Al-MCM-41 and Co/INT-MM1 samples because of these materials presented D_p similar values.

The low CO conversion and selectivity to C_{5+} observed for the Co/Al-MCM-41 solid compared to the Co/SBA-15 catalyst (see Table 2) could be attributed to the presence of aluminum in the MCM-41 structure. In spite of the fact that this element was introduced during the synthesis procedure of MCM-41 in order to improve its mechanical properties, it could significantly influence the reducibility degree of Co/Al-MCM-41 due to an increase of the metal-support interactions. Although to observe this effect largest amount of Al (>5 wt.%) should be added to the support [48].

4. Conclusions

The use of SBA-15 as cobalt catalyst support for the FTS seems to be very promising, since the Co/SBA-15 catalyst with a D_p of ~5 nm has shown the best catalytic behavior in comparison with the rest of the materials tested in reaction. Catalytic and characterization results have shown a great influence of mesoporous support porosity on the structure and reducibility of the cobalt oxide species formed inside the pores of the material during the calcining step. Characterization techniques have shown that the size of such supported species and their reducibility strongly depend on the D_p of mesoporous materials. Small pores of ~3 nm present in Al-MCM-41 and INT-MM1 lead to smaller supported Co clusters sizes with lower reducibility in H_2 and thus higher metal dispersions. Therefore, the surface-Co species located in the narrow pore silicas are less active and selective to long-chain hydrocarbons and more selective to CH_4 in FTS. Larger surface-Co species anchored or encapsulated in the wide pore mesoporous supports showed a contrary tendency.

Acknowledgments

The authors are grateful to PETROBRAS for the financial support of this research and to PDVSA–INTEVEP S.A., for providing the INT-MM1 mesoporous material. P. Navarro is grateful to the Spanish Ministry of Science and Innovation (MICINN) for financial support via "Juan de la Cierva" Programme.

References

[1] A. Khodakov, W. Chu, P. Fongarland, Chem. Rev. 107 (2007) 1692.
[2] J.H. Gregor, Catal. Lett. 7 (1990) 317.
[3] J.-S. Girardon, A. Constant-Griboval, L. Gengembre, P.A. Chernavskii, A.Y. Khodakov, Catal. Today 106 (2005) 161.
[4] G.P. Van der Laan, A.A.C.M. Beenackers, Catal. Rev. Sci. Eng. 41 (1999) 255.
[5] M.A. Vannice, J. Catal. 50 (1977) 228.
[6] E. Iglesia, Appl. Catal. A: Gen. 161 (1997) 59.
[7] A. Martínez, C. López, F. Márquez, I. Díaz, J. Catal. 220 (2003) 486.
[8] P. Concepción, C. López, A. Martínez, V.F. Puntes, J. Catal. 228 (2004) 321.
[9] R. Riva, H. Miesner, R. Vitali, G. Del Piero, Appl. Catal. A 196 (2000) 111.
[10] G. Boudjahem, S. Monteverdi, M. Mercy, M.M. Bettahar, J. Catal. 221 (2004) 325.
[11] T. Vrålstad, G. Øye, W.R. Rønning, M. Glomm, J. Stöcker, Sjöblom, Micropor. Mesopor. Mater. 80 (2005) 291.
[12] Y. Khodakov, V.L. Zholobenko, R. Bechara, D. Durand, Micropor. Mesopor. Mater. 79 (2005) 29.
[13] A. Jasik, R. Wojcieszak, S. Monteverdi, M. Ziolek, M.M. Bettahar, J. Mol. Catal. A 242 (2005) 81.
[14] Ø. Borg, S. Eri, E.A. Blekkan, S. Storsæter, H. Wigum, E. Rytter, A. Holmen, J. Catal. 248 (2007) 89.
[15] S. Storsæter, B. Tøtdal, J.C. Walmsley, B.S. Tanem, A. Holmen, J. Catal. 236 (2005) 139.
[16] T. Burakorn, J. Panpranot, O. Mekasuwandumrong, C. Chaisuk, P. Praserthdam, B. Jongsomjit, J. Mater. Process. Technol. 206 (1) (2008) 352.
[17] D. Xu, W. Li, H. Duan, Q. Ge, H. Xu, Catal. Lett. 102 (2005) 229.
[18] A.Y. Khodakov, A. Griboval-Constant, R. Bechara, F. Villian, J. Phys. Chem. B 105 (2001) 9805.
[19] R.C. Reuel, C.H. Bartholomew, J. Catal. 85 (1984) 63.
[20] A.Y. Khodakov, A. Griboval-Constant, R. Bechara, V.L. Zholobenko, J. Catal. 206 (2002) 230.
[21] R. Bechara, D. Balloy, D. Vanhove, Appl. Catal. A: Gen. 207 (2001) 343.
[22] G. Jacobs, T.K. Das, Y. Zhang, J. Li, G. Racoillet, B.H. Davis, Appl. Catal. A: Gen. 233 (2002) 263.
[23] Y. Ohtsuka, Y. Takahashi, M. Noguchi, T. Arai, S. Takasaki, N. Tsubouchi, Y. Wang, Catal. Today 89 (2004) 419.
[24] A. Martínez, C. López, Rev. Mex. Ing. Quím. 5 (2006) 167.
[25] Q. Tang, P. Wang, Q. Zhang, Y. Wang, Chem. Lett. 35 (4) (2006) 366.
[26] E. Lira, C.M. López, F. Oropeza, M. Bartolini, J. Alvarez, M.R. Goldwasser, F. López Linares, J.-F. Lamonier, M.J. Pérez Zurita, J. Mol. Catal. A: Chem. 281 (2008) 146.
[27] A. Griboval-Constant, A.Y. Khodakov, R. Bechara, V.L. Zholobenko, Stud. Surf. Sci. Catal. 144 (2002) 609.
[28] V.L. Zholobenko, A. Evans, D. Plant, S.M. Holmes, Micropor. Mesopor. Mater. 44–45 (2001) 793.
[29] D. Zhao, J. Sun, Q. Li, G.D. Stucky, Chem. Mater. 12 (2000) 275.
[30] D. Zhao, J. Feng, Q. Huo, N. Melosh, G.H. Fredrickson, B.F. Chmelka, G.D. Stucky, Science 279 (1998) 548.
[31] J. Carraza, J.R. Córdova, J. Lujano, J.M. Cruz, US Patent 5,840,271, November 24 (1998).
[32] O. González, J. Lujano, H. Molero, M. Pacheco, E. Pietri, M.R. Goldwasser, in: Proceedings of the 18th North American Catalysis Society Meeting, Cancún, México, June 1–6, (2003), p. 322.
[33] A. Hernández, J. Escobar, J.G. Pacheco, J.A. de los Reyes, M.C. Barrera, Rev. Soc. Quím. Méx. 48 (2004) 260.
[34] J.M. Kim, R. Ryoo, R. Bull, Korean Chem. Soc. 17 (1996) 66.
[35] B.D. Cullity, Elements of X-ray Diffraction, Addison–Wesley, London, 1978.
[36] A.M. Hilmen, D. Schanke, K.F. Hanssen, A. Holmen, Appl. Catal. A 186 (1999) 169.
[37] S. Vada, A. Hoff, E. Adnanes, D. Schanke, A. Holmen, Top. Catal. 2 (1995) 155.
[38] R.D. Jones, C.H. Bartholomew, Appl. Catal. 39 (1988) 77.

[39] L.C. Almeida, O. González, O. Sanz, A. Paul, M.A. Centeno, J.A. Odriozola, M. Montes, Stud. Surf. Sci. Catal. 167 (2007) 79.
[40] S. Brunauer, L.S. Deming, W.S. Deming, E. Teller, J. Am. Chem. Soc. 62 (1940) 1723.
[41] S.J. Gregg, K.S.W. Sing, Adsorption Surface Area and Porosity, second ed., Academic Press, London, 1982.
[42] Z. Luan, E.M. Maes, P.A.W. van der Heide, D. Zhao, R.S. Czernuszewicz, L. Kevan, Chem. Mater. 11 (1999) 3680.
[43] J.C. Groen, L.A.A. Peffer, J. Pérez-Ramírez, Micropor. Mesopor. Mater. 60 (2003) 1.
[44] S. Bessell, Appl. Catal. A 96 (1993) 253.
[45] S. Bessell, Appl. Catal. A 126 (1995) 235.
[46] A.Y. Khodakov, R. Bechara, A. Griboval-Constant, Appl. Catal. A: Gen. 254 (2003) 273.
[47] A.M. Saib, M. Claeys, E. van Steen, Catal. Today 71 (2002) 395.
[48] Y. Zhang, S. Nagamori, S. Hinchiranan, T. Vitidsant, N. Tsubaki, Energy & Fuels 20 (2) (2006) 417.
[49] C.N. Hamelinck, A. Faaij, H. den Uil, H. Boerrigter, Production of FT Transportation Fuels from Biomass, Technical Options, Process Analysis and Optimisation, and Development Potential, Netherlands Energy Research Foundation ECN and Utrecht University/Science, Technology and Society, Petten, Reports NWS-E-2003-08, 2003, 51 pp.